Title

Catalytic Ambient Temperature Dinitrogen Conversion to a Bis(silyl)amine by Mononuclear Group 4 Aryloxide Complexes

Journal

Inorganic Chemistry, 65(26)

ISSN

0020-1669

Authors

Hernandez, Matthew
Wong, Anthony
Lara, Jaden
et al.

Publication Date

2026-06-23

DOI

10.1021/acs.inorgchem.6c01010

Catalytic ambient temperature dinitrogen conversion to a bis(silyl)amine by mononuclear group 4 aryloxide complexes

Matthew Hernandez,[1] Anthony Wong,[1] Jaden Lara,[1] Shahbaz Ahmad,[2] Guodong Rao,[3] Nikolas Kaltsoyannis,[2] R. David Britt,[3] Polly L. Arnold*[1]

1. University of California, Berkeley, and Lawrence Berkeley National Laboratory; Berkeley, California CA 94720, US.

2. Department of Chemistry, University of Manchester, Oxford Road, Manchester M13 9PL, UK.

3. University of California, Davis; Davis, California CA 95616, US.

*Corresponding author. Email: pla@berkeley.edu.

Abstract

The homogeneous conversion of ambient dinitrogen to amine products via the N_2 reduction reaction (N_2RR) remains a prized yet challenging feat for d-block complexes and is scarcely reported for f-block complexes. New, mononuclear Ti^{IV} and Zr^{IV} aryloxide complexes $Ti(DP)_2$ (**1Ti**), $Zr(DP)_2$ (**1Zr**), and DP = [2-(OC_6H_2-2-^{t}Bu,4-$Me)_2$CHPh] produce up to 51 eq. and up to 7.0 eq. of $HN(SiMe_3)_2$ per Ti/Zr, from N_2, K^0, weak acid, and chlorotrimethylsilane. Complex **1Ti** exhibits more than double the activity toward N_2-silylation of any previously reported Ti N_2RR catalyst and can also catalyzes the formation of up to 19 eq. of NH_3, a new feature in early metal N_2RR chemistry. The mononuclear **1Zr** is the most active Zr catalyst for N_2-silylation to date. [$KSm(DP)_2(THF)_3$] (**1Sm**), the mononuclear analogue of our previously reported dinuclear **A-Sm** complex, displays only stoichiometric N_2-silylation due to its vulnerability to deleterious side-reactions. DFT calculations confirm the catalysis can proceed *via* a monomeric Ti complex with a terminally-bound, activated N_2, agreeing with experimental ^{1}H DOSY NMR measurements; the N-H bond is formed first, directing the catalyst selectivity. The isolable reduction product [K_3(THF)Ti(DP)(DP^-)(N_2)] is also an active catalyst, and an intermediate in the calculated cycle.

Introduction

The suite of homogeneous catalyst systems capable of reductive functionalization of dinitrogen, N_2RR, has expanded to include metals from across the periodic table.[1-6] While the first step in each system's catalytic cycle involves the formation of a metal-N_2 complex, the coordination geometry of these complexes is primarily dependent on the metal identity.[7, 8] The first isolable intermediate in the catalytic cycle typically consists of a mononuclear, end-on (η^1), terminally-bound N_2 adduct for mid- to late- d block metal complexes (chart 1c).[5, 9, 10] In contrast, the dinuclear bridging M-μ-N_2-M motif predominates in structurally characterized early transition metal and lanthanide N_2 adducts. Yet for electropositive metal (i.e. group 4 and rare-earth) complexes in particular, the preference for the N_2-coordination mode is less well-defined, and is still a topic of great interest.[11] All homogeneous N_2RR catalysts based on d-block complexes require an external source of reducing electrons which are most often provided by an alkali metal, in elemental or supported form (e.g. potassium graphite (KC_8), sodium amalgam (Na(Hg)), or potassium naphthalenide (KNaphth)). Catalysts based on early d- and f-block N_2RR systems require the external reductant to initiate N_2 binding, due to the lack of valence electrons available for back-donation to a weak π-acid.[12-14] These alkali metal cations brought from the reducing group 1 metal often play an important role in charge-stabilizing the anionic dinitrogen ligand.[15]

The number of complexes that can catalyze the ambient temperature and pressure conversion of N_2 to *tris*(trimethylsilyl)amine ($N(SiMe_3)_3$), or ammonia, using external reductant in the presence of Me_3SiCl electrophile or a weak acid respectively, is small but increasing. Efficient N-silylation requires slow reaction kinetics between reductant and electrophile.[2, 4, 6, 16] The tertiary silylamine is readily hydrolyzed to NH_3, however, its uses as a reagent in its own right remain somewhat limited to niche synthetic organic transformations.[9, 17-20]

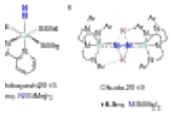

Chart 1a) The reductive transformation of dinitrogen to ammonia. b) reductive transformation of dinitrogen to *tris*(trimethylsilyl)amine. c) reductive transformation of dinitrogen to *bis*(trimethylsilyl)amine d) Mid d-block group 6 catalyst produces up to 1.8 eq. $HN(SiMe_3)_2$ alongside 3.2 eq. $N(SiMe_3)_3$ per Mo atom under N_2 with excess reductant and silyl electrophile. e) Representative late transition metal catalyst producing up to 36 eq. $N(SiMe_3)_3$ per Co atom, but no $HN(SiMe_3)_2$. f) Early transition metal catalyst producing up to 16.5 eq. $N(SiMe_3)_3$ per Ti atom.

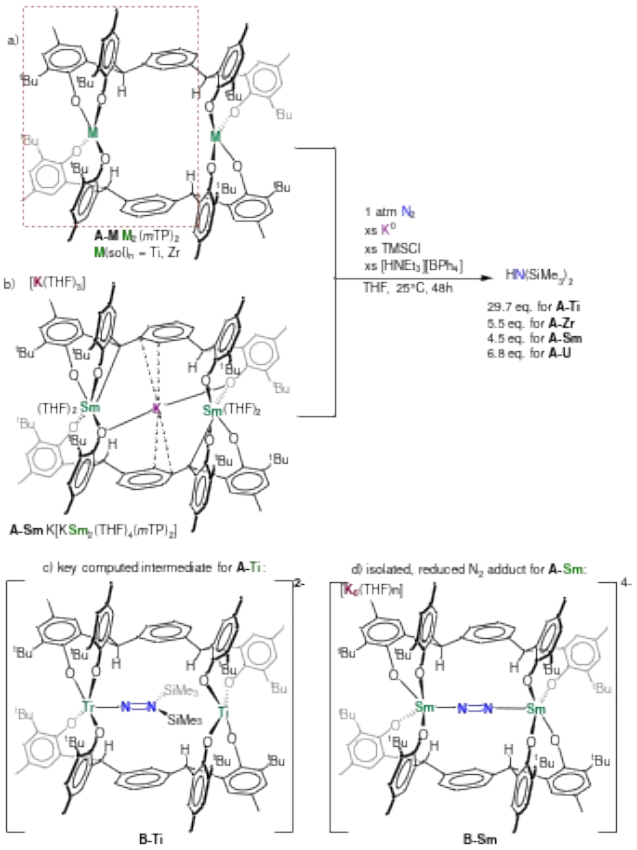

Scheme 1. a) Dinitrogen functionalization to secondary amines by group 4 and (b) lanthanide complexes by manipulation of the cavity size within the metallacyclic pocket. Inspiration for the mononuclear ligand is highlighted by the red box. c) a key intermediate in the Ti-catalyzed reaction, showing terminal, end-on coordination of N_2 d) The key intermediate in the Sm-catalyzed reductive silylation of N_2, showing the end-on bridging coordination mode.

Our group has previously established precedent for catalytic reductive dinitrogen silylation mediated by group 4, lanthanide, and actinide complexes **A-M** (Scheme 1a & 1b; $M_2(m\text{TP})_2$, M = Ti^{4+}, Zr^{4+}, U^{4+} or $K_2Ln_2(m\text{TP})_2(\text{THF})_{10}$, Ln = Sm^{3+}, Ce^{3+}) using a bridging tetraphenolate (*m*TP = [{2-(OC_6H_2-2-^{t}Bu,4-Me)$_2$CH}-1,3-C_6H_4])[21], wherein the space and accessibility of dinitrogen substrate binding is controlled by the metal identity and the ligand scaffold.[2, 6] The tetraphenolate proligand $m\text{TP}^{4-}$ bridges two metal centers and incorporates K^+ counter-cations that help stabilize reduced N_2-containing intermediates through π-interactions with the electron-rich arenes and dative bonds from O lone pairs.[22] When complexed with group 4 metals as $M_2(m\text{TP})_2$ (**A-M**, M = Ti, Zr, Scheme 1a) they active catalysts for the selective formation of $HN(SiMe_3)_2$. In this system, reactivity and DFT studies agreed that the reductive functionalization of the N_2 in the confined cavity in **A-Ti** enabled the catalytic conversion to $HN(SiMe_3)_2$ rather than $N(SiMe_3)_3$. This secondary silylamine exhibits greater synthetic versatility than its more conventionally generated tertiary counterpart, finding use as a precursor for sterically-hindered bases, itself as a reagent for silylation of alcohols, and in the chemical vapor deposition of silicon carbonitride thin films.[23-25] The computational work on the catalytic mechanism for **A-Ti** suggested that the N_2 remained bound through the α-N to only one of the two Ti centers during the catalysis (**B-Ti** in Scheme 1c), while the potassium counter-

cations within the metallacyclic cavity provided electrostatic stabilization of the β-N atom throughout the reductive functionalization steps.

In contrast, the f-block $K_2Ln_2(mTP)_2(THF)_{10}$, and THF-solvated $\{U(THF)_2\}_2(mTP)_2$ (**A-Ln,** Ln = Sm^{3+}, Ce^{3+}, **A-U**) can also make tris(silyl)amine from N_2, which we attributed to the larger and more flexible cavity. Although a detailed mechanism for the selective N_2RR catalyzed by the lanthanide analogues (**A-Ln)** hadn't yet been elucidated, an end-on $Sm(\eta^1{:}\eta^1\text{-}\mu\text{-}N_2)Sm$ (**B-Sm**) was characterized, and we have since provided a DFT-computed mechanism for conversion of N_2 to $N(SiMe_3)_3$ that agrees with this binding mode.[2, 6, 26]

Experimental confirmation of our theoretical study on N_2-silylation mediated by **A-Ti** would invoke a mononuclear, terminal Ti-N_2 adduct. Terminally bound Ti-N_2 adducts have been reported (Chart 2), but most equilibrate between different N_2-coordination modes, and none thus far are competent for catalytic N_2 functionalization.[27] The N_2 binding in these instances was characterized by UV-vis, NMR, and IR spectroscopies, and the 2004 example reported by Chirik et al. (Chart 2a) releases stoichiometric quantities of H_2, N_2 and $N_2H_4{\cdot}2HCl$ upon treatment with HCl at -80°C. [28, 29] We hypothesized that a mononuclear metal-aryloxide complex with the capacity to incorporate stabilizing K^+ counter-cations into the scaffold could demonstrate similar reactivity to its dinuclear analogue. We hoped this simpler system, essentially half of the original tetraphenolate complex (Scheme 1a), could help determine whether a second redox-active metal center is required for catalytic N_2 silylation by group 4 metal and Ln-complexes.

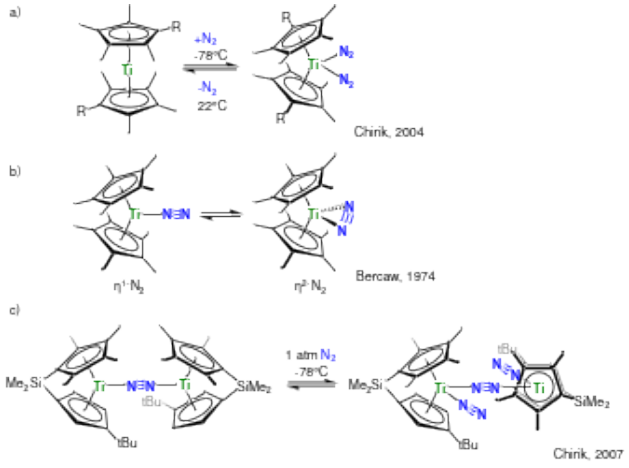

Chart 2 a) Temperature-dependent equilibration between terminal end-on and side-on titanocene-dinitrogen complex, with η^1 favored at higher temperatures. b) Temperature-dependent coordination of dinitrogen at titanocene-derivative complexes. c) Temperature-dependence on the coordination environment of a dinuclear titanocene-N_2 complex.

Here, we show that homoleptic, mononuclear metal-diphenolate complexes (**1M**) can effect catalytic transformation of N_2 to $HN(SiMe_3)_2$ in the presence of reductant (K^0), weak acid ($[HNEt_3][BPh_4]$), and electrophile (Me_3SiCl) at ambient temperature and pressure for M = Ti and Zr, but not

for Sm. Measurements from ^{1}H DOSY NMR, EPR spectroscopy, and DFT calculations agree that these complexes remain mononuclear upon reductive N_2 binding and functionalization, representing a noteworthy departure from the bridging coordination mode typically observed for group 4 metal-based N_2RR catalysts. [30,31] Selectivity for the secondary silylamine is a unique feature of our previous metal-aryloxide-based catalyst systems that is preserved in the present study, providing a viable route to a chemical frequently encountered in synthetic laboratories. We also show that **1Ti** can produce up to 19 eq. NH_3 (Table S2, entry 2) under similar conditions with omission of the silyl electrophile, demonstrating the first example of an N_2RR catalyst capable of selectively producing either $HN(SiMe_3)_2$ or NH_3. The robustness of **1Ti** is again highlighted by its resistance to decomposition over multiple batch recharges of catalytic reagents (Table S1), furthering its utility as a catalyst for the reductive transformation of dinitrogen.

Results and Discussion

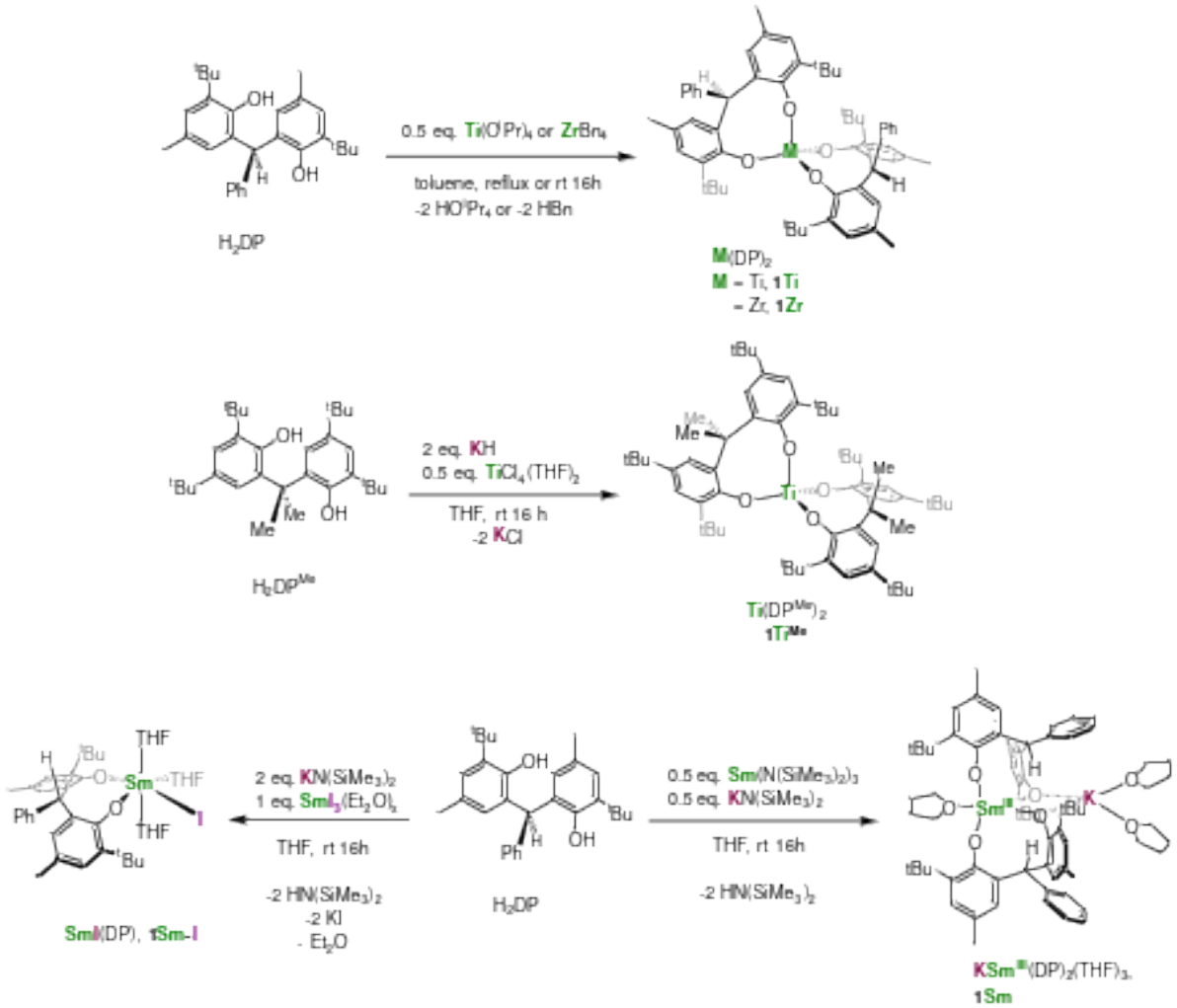

Scheme 2 Synthetic routes to the precatalysts used for N_2RR in this work.

The diphenol H_2DP (HOC_6H_2-^{t}Bu-2,Me-4)$_2$CHPh can be prepared in one pot with inexpensive, commercially available reagents in 60 % yield. Metalation via protonolysis or salt-elimination pathways (vide infra, *Syntheses*) furnishes the new, fully characterized complexes **1Ti**, **1Zr**, **1Sm**, and **1Sm-I** in good yields (Figure 1). While the group 4 complexes are soluble in hydrocarbon and ethereal solvents, the -ate complex **1Sm** is sparingly soluble in THF but dissolves in pyridine. The ^{1}H NMR spectra of **1Ti** and **1Zr** show two sets of methyl- and *tert*-butyl resonances assigned to a rigid, *pseudo*-tetrahedral coordination geometry around the central metal cations, in agreement with the solid-state structure (SCXRD) shown in Figure 1a, 2b. The toluene adduct of **1Sm**, **1Sm-tol,** has a similar solid-state structure (Figure 1c) but the corresponding resonances for solutions of **1Sm** are equivalent on the ^{1}H NMR timescale, in agreement with the larger ionic radius of the Sm^{III} center and greater flexibility of the ligand coordination.[32] We also made the heteroleptic **1Sm-I**, hypothesizing that elimination of the iodide upon reduction could facilitate N_2-binding; the solid-state structure is shown in Figure 1d.

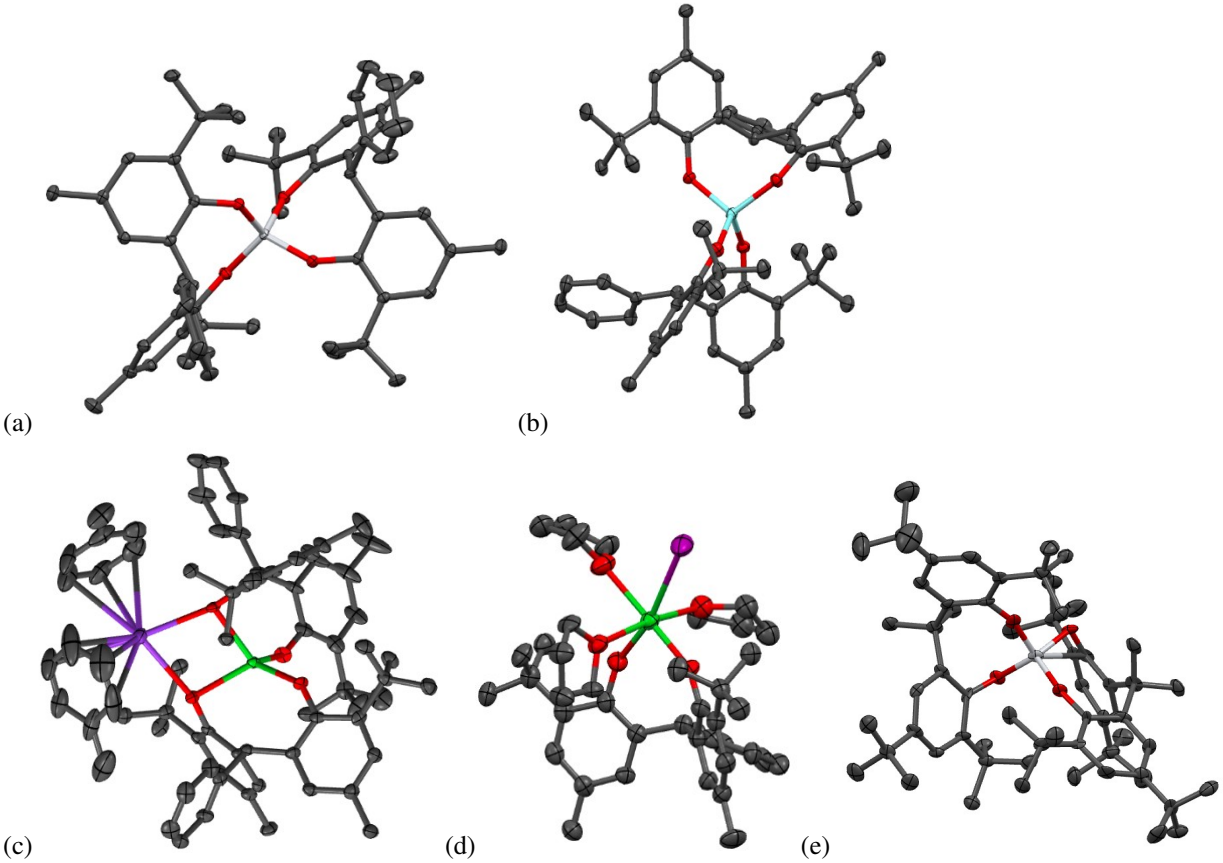

Figure 1 Solid-state structures of the N_2RR catalysts (a) **1Ti**, (b) **1Zr,** (c) **1Sm-tol** and (d) **1Sm-I**. Solid-state structural data for (e) **1Ti^{Me}** is of poor quality and is shown only for connectivity. Selected distances (Å) and angles (°): Average Ti-O bond length in **1Ti** = 1.809(6) Å, average Zr-O bond length in **1Zr** = 1.954(2) Å, average Sm-O bond length in **1Sm-tol** = 2.224(3) Å, and Sm-I bond length in **1Sm-I** = 3.105(1) Å. Probability ellipsoids set at 50 %, H and lattice solvent atoms omitted for clarity. Color key: white = Ti, turquoise = Zr; green = Sm; purple = K; red = O; grey = C.

Catalytic conversion of N_2 to $HN(SiMe_3)_2$

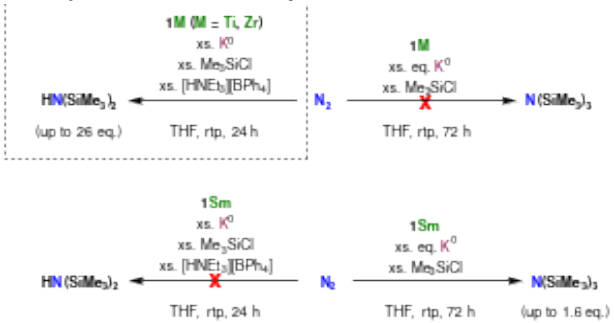

Scheme 3 Various conditions employed for N_2RR using the mononuclear group 4 and Ln complexes **1M** (M = Ti, Ti^{Me}, Zr, Sm, Sm-I) using K^0 as reductant, trimethylchlorosilane as electrophile, and a weak acid. rtp = room temperature and pressure; xs. = excess. The highlighted reaction generates catalytic product yields.

We tested these novel mononuclear complexes for the ambient conversion of N_2 to *bis*(trimethylsilyl)amine, $HN(SiMe_3)_2$, and *tris*(trimethylsilyl)amine, $N(SiMe_3)_3$, under the same reaction conditions as used with our previously reported bimetallic catalysts (Scheme 3). The reaction mixture comprises a THF solution of the precatalyst (**1M**, **M = Ti, Zr, Sm, Sm-I**) sealed in a Schlenk flask under 1 atm N_2 in the presence of a solid piece of potassium metal reductant, an excess chlorotrimethylsilane (Me_3SiCl), and, according to the entry in Table 1, an excess of $[HNEt_3][BPh_4]$ all stirred vigorously with a glass-covered stir-bar. As mentioned, K^0 was chosen as the preferred reductant rather than KC_8, due to its slower background reactions with the other reagents. Alternative proton sources were screened ([HDBU][BPh_4], 2,4,6-tri-*tert*-butylphenol, and ^{t}BuOH), but reactions employing the triethylammonium salt consistently perform best. Inclusion or omission of H^+ allowed us to target formation of the 2° or 3° silylamine, respectively. After 24 hours the volatile components in the reaction mixture are collected by trap-to-trap vacuum transfer and analyzed by gas chromatography, ^{1}H, and ^{29}Si NMR spectroscopies (figures S39-S43).

Table 1 Conversion of N_2 to silylamines by the mono- and dinuclear aryloxide complexes under ambient conditions (1 atm N_2, room temperature) with 300 eq. K^0 as reductant. "Equivalents" reported correspond to (mol product)/(mol precatalyst). This number also conveniently corresponds to the percent yield with respect to reducing electrons added; for example, 30 eq. silylamine = 30% yield. All catalytic yields (≥ 2 eq.) of silylamine are reported as an average of triplicate experiments with standard error. Reaction mixtures including H^+ were allowed to stir at room temperature for 24 hours before distilling out the products, while those omitting H^+ stirred for 72 hours.

Entry	Precatalyst[a]	Me_3SiCl (eq.)	$[HNEt_3][BPh_4]$ (eq.)	$HN(SiMe_3)_2$ (eq.)	$N(SiMe_3)_3$ (eq.)
1	**1Ti**	225	131	26 ± 2	4.0 ± 1.2
2	**1Ti**	300	0	-	0.61
3	**A-Ti**[a]	225	131	30 ± 1	5.4 ± 0.5
4	**A-Ti**[a]	300	0	-	1.4
5	**$1Ti^{Me}$**	225	131	34 ± 2	3.1 ± 2.2

6	**1Ti^{Me}**	300	0	-	0.59
7	**1Zr**	225	131	7.0 ± 0.8	1.4 ± 0.3
8	**1Zr**	300	0	-	0
9	**A-Zr**[a]	225	131	5.5 ± 0.4	2.7 ± 1.6
10	**A-Zr**[a]	300	0	-	0.62
11	**1Sm**	225	131	0	0
12	**1Sm**	300	0	-	1.6
13	**A-Sm**[a]	225	131	3.7 ± 0.6	0
14	**A-Sm**[a]	300	0	-	5.4 ± 0.8
15	**1Sm-I**	300	0	-	1.4
16	**A-Sm-I**[a]	300	0	-	2.8 ± 0.2
17	**1Ti**[b]	225 (4x)	131 (4x)	51	5.1
18	**A-Ti**[a,b]	225 (4x)	131 (4x)	76	8.2

a) Values reported from previous study.[2] b) Silylamine yields are the cumulative result from 4 consecutive catalytic N_2 silylation reactions, see page S17 for details. Equivalents are not reported in triplicate for these entries.

Most notably, like their dinuclear analogues **A-M**, mononuclear group 4 **1M** complexes only catalyze conversion of N_2 to $HN(SiMe_3)_2$; neither is competent for catalytic $N(SiMe_3)_3$ production under our conditions. $HN(SiMe_3)_2$ is the only product released from the catalytic cycle for **1Ti** and **1Zr**; we have previously determined that the quantities of 3° silylamine reported in Table 1 result from the reaction of $HN(SiMe_3)_2$ with K^0 and Me_3SiCl.[2]

Subjecting **1Ti** (table 1, entry 1) to the same catalytic reaction conditions as its dinuclear analogue, **A-Ti** (table 1, entry 3), gives nearly identical upper limits for total silylamine yield (36 eq. vs. 35 eq.) and selectivity (82% vs. 85%) for $HN(SiMe_3)_2$, experimentally corroborating the DFT-calculated mechanism for reductive N_2 functionalization at a single Ti center in **A-Ti**. The equivalents of product is effectively doubled with respect to the number of Ti atoms. Like **A-Ti**, **1Ti** only catalyzes the conversion of N_2 to $HN(SiMe_3)_2$ when a H^+ source is included (table 1, entry 2). We infer that the smaller ionic radius of the 3d metal increases the steric influence of the ligands on the bound N_2 and prevents a third N-silylation, even outside the formal cavity employed by **A-Ti**. DFT calculations support this inference, (*vide infra,* figure 2) invoking protonation of the distal N atom as the first electrophilic functionalization.[33] Our previous kinetic studies of **A-Ti** and **A-U** all confirm that $HN(SiMe_3)_2$ is the product of these aryloxide-supported electropositive-metal-mediated N_2RRs, and it is a subsequent reaction of this product with the K and TMSCl in solution that form the $N(SiMe_3)_3$ byproduct at later stages in the reaction.[2] **1Ti** strikes a lucrative balance between reactivity toward N_2 and stability toward our catalytic reagents. It is sufficiently robust to withstand exposure to large excesses of electrophiles, as well as the elevated temperatures and reduced pressures associated with amine product collection. The catalyst even continues to function effectively over four consecutive additions of additional substrate and reagents (table 1, entry 17), yielding a maximum of 56 eq. amine per Ti catalyst for **1Ti**. The product yield steadily decreased after each catalytic cycle, amounting to a 14.0% total yield with respect to reducing equivalents, but whether that decrease is attributed to catalyst decomposition or incomplete post-run extraction is

difficult to rigorously determine (figure S22). We also measure up to 19 eq. of NH_3 (scheme 4) by ^1H NMR (figure S23) when subjecting **1Ti** to excess K^0 and H^+, making **1Ti** the first reported complex to demonstrate efficacy in the transformation of N_2 to both $HN(SiMe_3)_2$ and NH_3. This result is consistent with the possibility that, under otherwise similar reducing and protonating conditions but in the absence of TMSCl, protonated N-containing intermediates within the catalytic manifold are diverted away from N-silylation and instead proceed through further protonation/reduction to NH_3.

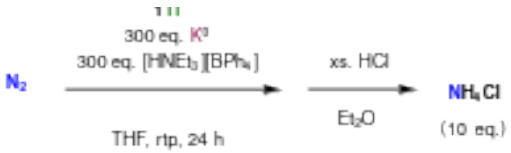

Scheme 4. Catalytic NH_3 production by **1Ti**.

To determine the value of the benzylic C-H in the DP ligands on **1Ti** (*vide infra*, scheme 5), we synthesized the methylated analogue $Ti\{(OC_6H_2\text{-}^tBu\text{-}2,Me\text{-}4)_2CMe_2\}_2$ **1Ti^{Me}** via salt metathesis (*vide infra*, Syntheses) from the proligand, **H$_2$DP^{Me}**[34], wherein two methyl groups replace the –H and –Ph substituents at the methylene bridge. This substitution precludes opportunity for deprotonation and subsequent metalation at the acidic, benzylic position on the ligand in the presence of excess reductant and thus was posited to give higher silylamine yield. **1Ti^{Me}** is similarly competent for $HN(SiMe_3)_2$ production as **1Ti** under catalytic conditions, giving 30 eq. 2° silylamine (table 1, entry 5). Targeting the 3° silylamine by omission of H^+ from the reagents again gives sub-stoichiometric conversion (table 1, entry 6). However, the complex is much less robust than the parent **1Ti** and all reactions targeting a **1Ti^{Me}**-N_2 adduct, by KC_8 or K^0 reduction of **1Ti^{Me}** in THF at -78°C, result in complete decomposition and release of the potassium salt of the ligand, **K$_2$DP^{Me}** (Figure S34), hindering further study.

Cyclic voltammetry studies on solutions of **1M** show negative reduction potentials for all three, anticipated given the strong donation from the aryloxide ligands raising the energy of a metal-centered LUMO. **1Ti** outperforms **1Zr**, possibly due to the difference in reduction potentials (Figures S1 and S2) of the two tetravalent metal centers, which is valuable in N_2 binding. A reversible one-electron electrochemical reduction wave attributed to the $M^{4+/3+}$ couple was measured at -1.82 V vs. Fc^+ for **1Ti**, and an irreversible wave at -3.1 V vs. $Fc^{0/+}$ for **1Zr**. No reduction was observed within the THF solvent window (above -3.3 V vs. $Fc^{0/+}$) for the Sm precatalysts (**1Sm**, and **1Sm-I**).

Another contributing factor for the performance differences of **1Ti**, **1Zr** and **1Sm** can also be explained by the catalytic mixture's (**1M +** N_2 + K^0 in THF) tendency to decompose in the presence of the acid $[HNEt_3][BPh_4]$. For **1Zr**, a mixture of these reagents in d_8-THF in a Young's tap-fitted NMR tube shows partial conversion to **H$_2$DP** (Figure S26). In contrast, the **1Ti** mixture demonstrates almost no decomposition to **H$_2$DP** under the same conditions (Figure S25).

Nonetheless, **1Zr** is a catalyst for production of the 2° silylamine (7.0 eq.) formation, table 1, entry 7), and to our knowledge is the most active zirconium-N_2RR catalyst reported so far, even outperforming its dinuclear analogue **A-Zr** (table 1, entry 9). The third N-silylation event to generate the 3° amine, however, is still inaccessible for the 4d cation (table 1, entry 10), emphasizing the steric requirements at the metal for a third N-silylation event. The mixture of **1Sm** + N_2 + K^0 quickly decomposes upon treatment with [$HNEt_3$][BPh_4] to release **H_2DP** (Figure S27), preventing the conversion of any bound N_2 to $HN(SiMe_3)_2$ (table 1, entry 11). This is a significant decrease in kinetic inertness compared to the dinuclear analogue **A-Sm**, which was able to make 3.7 eq. of $HN(SiMe_3)_2$ under these reaction conditions. The sub-stoichiometric yield of 1.6 eq. of $N(SiMe_3)_3$ by **1Sm** (table 1, entry 12) is also substantially lower than that observed for **A-Sm** which produces up to 5.4 eq. $N(SiMe_3)_3$. The heteroleptic **1Sm-I** (table 1, entry 13) performs similarly to **1Sm** giving sub-stoichiometric conversion of N_2 to the 3° silylamine (1.40 equivs $N(SiMe_3)_3$). We also measure a decreased yield with **1Sm-I** relative to its dinuclear counterpart **B-Sm** $K_2Sm_2(mTP)_2(THF)_{10,}$ (table 1, entry 16). Nonetheless, the lanthanide congeners are the only complexes evaluated capable of facilitating production of the 3° silylamine in near-stoichiometric yields.

Studies of the products of reduction of 1M under N_2

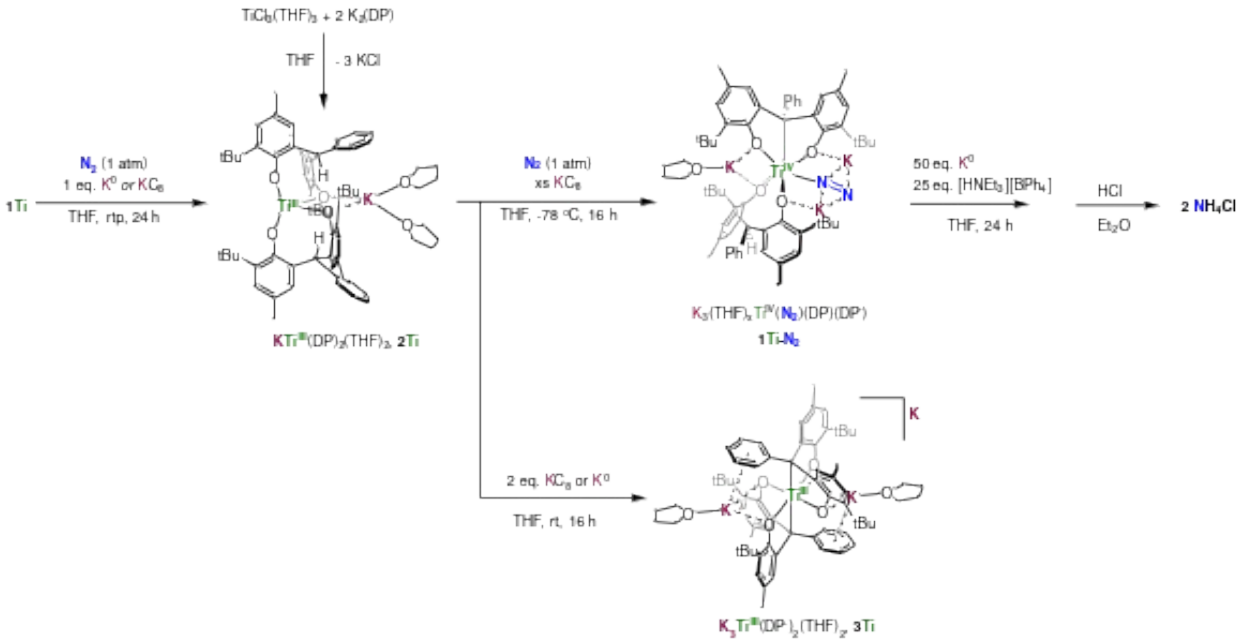

Scheme 5. Reduction of **1Ti** with KC_8 under N_2 in the absence of protons or electrophile to make reduced, N_2-containing **1Ti-N_2**. Subsequent quench with additional equivalents of reducing electrons and H^+ releases NH_3 which can be protonated and quantified by ^1H NMR. Reduction of **2Ti** in the absence of N_2 produces **3Ti**. Precise locations and solvation of the K^+ counterions are solvent-dependent.

We endeavored to isolate a metal-N_2 adduct en route to the silylamine product that could provide more information about the intermediate(s). While K^0 was the reductant evaluated for catalytic silylation reactions, KC_8 was preferred for studying the N_2-adduct for several reasons discussed in greater detail below.

We characterize the major product formed from the reduction of **1Ti** under N_2 in THF at -78°C with excess (greater than 3 eq.) KC_8 as $[K_3(THF)][Ti^{IV}(N_2)(DP)(DP^-)]$ **1Ti-N_2** wherein one DP ligand has been deprotonated and metalated at the benzylic position (Scheme 5). After isolation as a dark red solid, the compound is stable at room temperature under an N_2 atmosphere. We suggest the reaction proceeds via an initial $1e^-$ reduction to $[K(THF)_n][Ti^{III}(DP)_2]$, **2Ti**. This is because **1Ti-N_2** can also be formed by KC_8 reduction of **2Ti** which itself can be independently synthesized from $Ti^{III}Cl_3(THF)_3$ (see SI). Treatment of this material with a THF solution of $[DNEt_3][BPh_4]$ followed by filtration through silica gel with $CDCl_3$ reveals 43% deuteration by ^1H NMR suggesting one of the two ligands has been deprotonated at the benzylic carbon (Figures S21 and S22). A desymmetrized ligand set is reflected in both the integration and number of distinct ^1H NMR resonances. Complex **1Ti-N_2** displays ^1H NMR spectra consistent with a diamagnetic complex while X-band CW EPR shows no features that would be attributable to a paramagnetic Ti^{III} complex (g = 2.003, figure S44). Evans method NMR spectroscopic determination of solution

paramagnetism further confirms the absence of Ti^{III}.[35] A stoichiometric quantity of NH_3 (2.2 eq. as NH_4Cl per mol precatalyst) is formed from reduction of **2Ti** under N_2 with excess KC_8 at -78°C to form **1Ti-N_2,** followed by quench with $[HNEt_3][BPh_4]$ in the presence of K^0 to supply the additional e^- required to complete N-N bond cleavage (Table S2). We recover a similar yield (1.8 eq. $^{14}NH_4Cl$ + $^{15}NH_4Cl$) when performing this reaction on **1Ti-$^{15}N_2$** (Figure S36). This 1:2 Ti:N ratio supports formulation of **1Ti-N_2** as a mononuclear N_2 complex, and is further confirmed by a ^{1}H DOSY NMR spectroscopic study (Table S4). Because the diffusion coefficient (D) is inversely correlated with molecular weight, the nuclearity of **1Ti–N_2** is inferred by comparison with complexes of related composition. The diffusion coefficient of **1Ti–N_2** ($D = 6.89 \times 10^{-10}$ m^2s^{-1}) is comparable to those of **1Ti** ($D = 6.89 \times 10^{-10}$ m^2 s^{-1}) and **3Ti** ($D = 6.02 \times 10^{-10}$ m^2s^{-1}), and significantly greater than that of **A-K_4Ti** ($D = 4.70 \times 10^{-10}$ m^2s^{-1}), which serves as a representative di-titanium the 2:2 metal:ligand complex. Accordingly, we characterize **1Ti–N_2** as a monomeric complex in solution. This is an interesting finding, as all previously isolated and characterized examples of homogeneous group 4 metal- and lanthanide-mediated catalytic N_2RR feature a $(\mu\text{-}N_2)^{n-}$ unit ligated between two redox-active metal centers.[11, 12, 36-41] Here, N_2-silylation yields, ^{1}H DOSY NMR and DFT calculations (*vide infra*) all support the formulation of a terminally-bound N_2 ligand to a single Ti atom (Figure 2). The calculated starting point of the catalytic cycle, intermediate **I**, corresponds to the non-deprotonated three-electron-reduced species **1Ti-N_2'**, whereas the isolated complex **1Ti-N_2** is its benzylically deprotonated analogue. Numerous attempts to grow crystals suitable for SCXRD were unsuccessful, and **1Ti-N_2** is too sensitive for both electrospray ionization (ESI) and MALDI mass spectrometry measurements in our instruments. We also attempted stoichiometric, electrophilic functionalization of the N_2 moiety in **1Ti-N_2** with various reagents to trap and characterize a catalytic intermediate, though none were successful. However, subjecting a THF solution of **1Ti-N_2** to excess K^0, Me_3SiCl, and $[HNEt_3][BPh_4]$ results in catalytic production of 2° silylamine (14 eq.), supporting our positioning of this complex as a catalytically competent, experimentally accessible species that can re-enter the catalytic manifold. Elemental analysis of **1Ti-N_2** returns erroneously low values for C, H, and N, emphasizing the highly unstable nature of these catalytic intermediates.

Conversely, when THF solutions of either **1Ti** or **2Ti** are treated with excess K^0 at -78°C, no reaction is observed on a reasonable timescale. Slow warming of either reaction mixture to room temperature results in the formation of a product mixture we denote as **2Ti-N_2** that consists of **1Ti-N_2, 3Ti**, and an uncharacterized Ti^{III} species**.** Large brown blocks of **3Ti** can be recovered by diffusion of hexane vapor into a concentrated THF solution of **2Ti-N_2** but we struggled to thoroughly separate the remaining products, hence most of the characterization efforts were focused on **1Ti-N_2** (the product of -78°C reductions with KC_8). X-band EPR measurements on the mother liquor of **2Ti-N_2** after crystallizations to remove **3Ti** reveal the signature of the unidentified Ti^{III} species (g = [1.97, 1.94, 1.89] figure S44). Our previous study of the N_2 silylation catalyzed by **A-Ti** suggested that dehydrometalated Ti complexes, formed via reductive deprotonation of a close benzylic C-H by a transient Ti^{II} center, lacked adequate space to reductively bind N_2 at the Ti center. Thus, H^+ was required to liberate the N_2 coordination site and re-enter the catalytic cycle. Although

3Ti forms as a by-product from the treatment of **1Ti** with K^0 at room temperature in the mononuclear system, we similarly hypothesize here that the presence of H^+ in the reaction solution reprotonates the ligand's benzylic position to bring the complex back into the catalytic cycle. This hypothesis is supported by the catalytic yields of $HN(SiMe_3)_2$ (14 eq.) obtained from the reaction between **3Ti** and excess K^0, $[HNEt_3][BPh_4]$, and TMSCl. Nonetheless, a decreased yield of NH_4Cl (1.4 eq.) is obtained from a quench with additional K^0 and $[HNEt_3][BPh_4]$ due to the presence of additional species in the mixture that do not contribute to the reductive functionalization of N_2.

The same procedure with **1Sm** to form NH_3 (THF slurry of precatalyst with KC_8 at -78°C under N_2 followed by K^0 and $[HNEt_3][BPh_4]$) yields 0.043 eq. NH_4Cl relative to **1Sm** (Figure S38), but the extreme air sensitivity of the system precluded attempts to isolate any reduction intermediates.

Vibrational Spectroscopy

We anticipated that vibrational spectroscopy would aid in characterization of **1Ti-N_2**. After reduction of **1Ti** with excess KC_8 under an atmosphere of N_2 at -78°C, a broad feature at 1571 cm^{-1} appears in the ATR-FTIR spectra of a sample of the solid material which is within reasonable range of literature values reported for moderately activated N_2 ligands. [42-44,28, 45] Upon treatment of a THF solution of **1Ti** with $[HNEt_3][BPh_4]$ and TMSCl the intensity of the IR feature substantially decreases, confirming consumption of the starting material (Figure S45). Unfortunately, efforts to compare the vibrational properties of **1Ti-$^{14}N_2$** and **1Ti-$^{15}N_2$** by both Raman and IR spectroscopies were unsuccessful, attributed to the weak oscillator strength of the N-N vibration in these complexes.

DFT-proposed mechanism for Ti-mediated catalytic N_2 silylation

DFT calculations were performed to elucidate the mechanism for catalytic N_2-silylation mediated by **1Ti**. Computational details are provided in full in the ESI under the section "Computational Methods" (page S48). A key vibrational feature at 1577 cm^{-1} was assigned to the three-electron-reduced species **1Ti-N_2**, rather than to its singly or doubly reduced precursors (Fig. S49). This species, denoted as intermediate (**a**) (**I** in Figure S51), was identified as the starting point of the catalytic cycle, consistent with experimental IR data. Formation of a dinuclear, μ-N_2 intermediate from **I** was evaluated but found to be less thermodynamically favorable than its protonation. Because some elementary steps can involve ion-pairing/association or charge-separated species, our mechanistic conclusions are based primarily on internally consistent relative comparisons of ΔG and $\Delta G^{\ddagger}$ between competing pathways computed with the same protocol.

Nine possible reaction pathways (**A**–**I**) were evaluated to determine the most viable route for dinitrogen reduction and functionalization under the given experimental conditions; the full set of competing pathways is provided in the ESI (Figure S51). Comparison of the computed Gibbs free energy profiles and kinetic barriers identified **pathway F** as the most favorable, and it is therefore

the pathway discussed here and shown in **Figure 2**. This catalytic pathway initiates with a protonation step, where a proton donor, $[HNEt_3][BPh_4]$, transfers its proton to the terminal nitrogen of the **1Ti-N$_2$** (**a**) (**I** in Figure S51) complex, leading to **K$_2$[Ti^{III}DP$_2$(N)N^H]** (**b**) (**I** in Figure S51). During efforts to model this proton transfer, optimization of the corresponding encounter reactant complex proceeded directly to the protonated product rather than to a stable pre-protonation minimum; on this basis, within our DFT protocol, protonation is treated as effectively barrierless and was therefore taken as the initiating event in each half of the catalytic cycle. This step, which replaces a potassium cation with a proton, is highly exergonic (ΔG = –24.8 kcal mol^{-1}), demonstrating a strong thermodynamic driving force, and directs the catalyst selectivity.

Following protonation, the reaction proceeds through a concerted reduction and trimethylsilyl chloride (TMSCl) uptake step, wherein an additional electron is transferred to the titanium center, enabling nucleophilic attack on TMSCl. This transformation yields the silylated intermediate **K$_2$[Ti^{III}DP$_2$(N)N^{H}TMS]** (**c**) (**IX** in Figure S51), with a moderate kinetic barrier of 11.0 kcal mol^{-1}, which is readily surmountable at ambient temperature and is strongly exergonic, with a thermodynamic driving force of –41.1 kcal mol^{-1}. This order of functionalization is chemically reasonable because protonation occurs first at the distal N atom, which is the less sterically hindered and more accessible site for subsequent silylation, and is consistent with the observed formation and release of $HN(SiMe_3)_2$ rather than pathways leading to disilylhydrazine formation. Within the proposed mechanism, the reduction/TMSCl uptake step from (**a**) to (**c**) is the stage at which TMSCl likely diverts the reaction pathway toward N-silylation, whereas in its absence the protonated N-containing intermediate could instead undergo further protonation/reduction toward NH_3 formation. A subsequent reduction and silylation event results in **K$_2$[Ti^{III}DP$_2$(N)N^{H}TMS$_2$]** (**d**) (**IV** in Figure S51), which releases –11.6 kcal mol^{-1} in Gibbs energy *via* an activation barrier of 18.8 kcal mol^{-1}, surmountable under standard laboratory conditions.

A critical transformation in the catalytic cycle occurs with product elimination, where the silylated secondary amine $HN(SiMe_3)_2$ dissociates from **K$_2$[Ti^{III}DP$_2$(N)N^{H}TMS$_2$]** (**d**), generating **K$_3$[Ti^{III}DP$_2$(N)]** (**e**) (**V** in Figure S51). This step is highly exergonic (ΔG = –64.8 kcal mol^{-1}), indicating that product release is a major driving force sustaining the catalytic cycle. Notably, the presence of potassium counterions is crucial in stabilizing the reduced nitrogen-containing intermediates throughout the process, as computational results suggest that potassium engages in electrostatic interactions that facilitate electron transfer and structural stabilization.

The second half of the catalytic sequence follows a similar pattern, starting with a second protonation event at the titanium-bound nitrogen, forming **K$_2$[Ti^{III}DP$_2$(N^H)]** (**f**) (**X** in Figure S51) (ΔG = –42.4 kcal mol^{-1}). A subsequent concerted reduction and TMSCl uptake step converts **K$_2$[Ti^{III}DP$_2$(N^H)]** (**f**) into **K$_2$[Ti^{III}DP$_2$(N^{H}TMS)]** (**g**) (**XI** in Figure S51), accompanied by a substantial driving force (ΔG = –98.4 kcal mol^{-1}). Finally, dinitrogen coordination and reduction

restore the initial catalytic species **$K_3[Ti^{III}DP_2(N_2)]$** (**a**), completing the cycle and giving ΔG = –60.8 kcal mol^{-1}.

Finally, the formation of a dinuclear intermediate from **1Ti-N_2'** was also computationally explored, see page S50 for details. The formation of a dinuclear intermediate was found to have a driving force of –18.8 kcal mol^{-1}, which is 5.8 kcal mol^{-1} less favorable compared to the protonation step at the mononuclear complex. Given that protonation occurs spontaneously without an activation barrier and is more favorable thermodynamically, the computational data clearly support a mononuclear pathway.

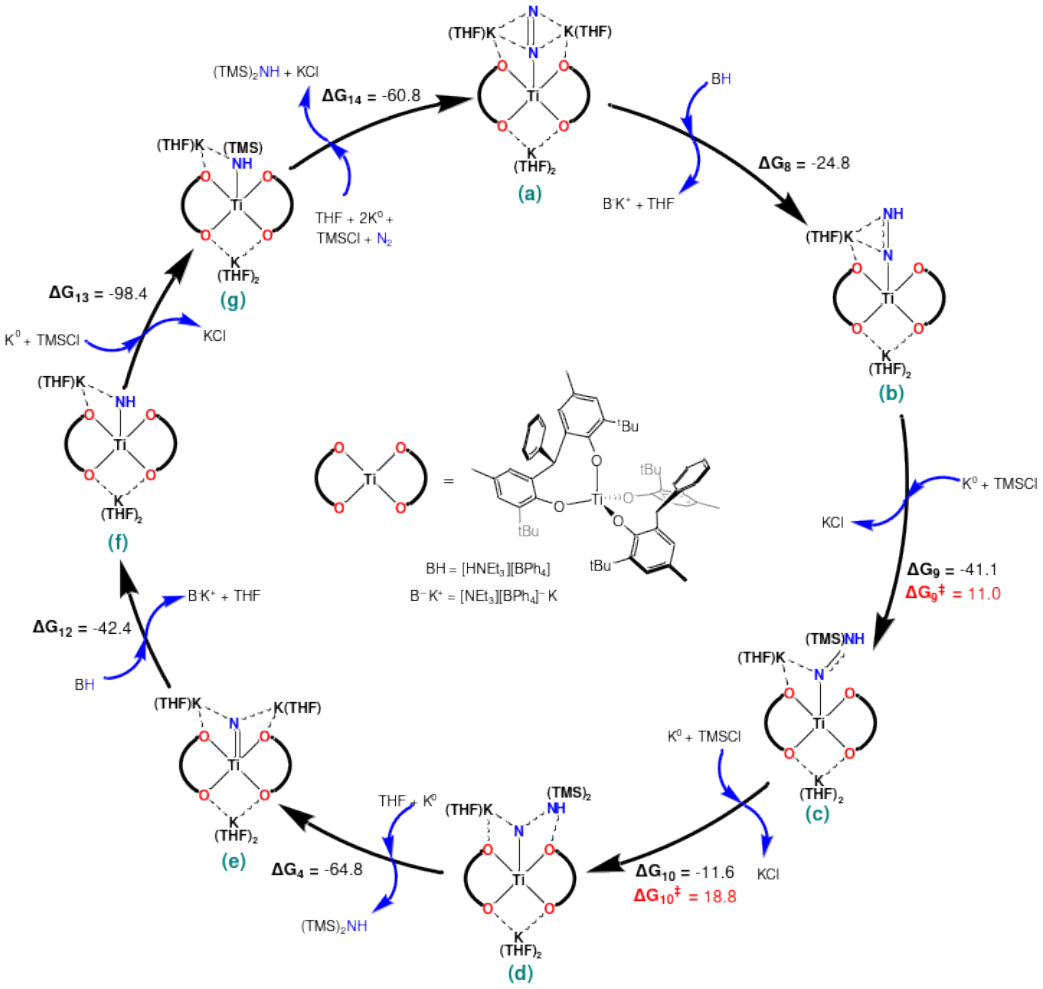

Figure 2 a) Calculated mechanistic **pathway F** for titanium-catalyzed dinitrogen functionalization. Free energies (in kcal mol^{-1}) and bond orders, determined using Wiberg bond indices, were both calculated at the PBE0-D3BJ/BS2/SMD // PBE0-D3BJ/BS1 level of theory. TMS = Me_3Si. Full computational details and the full comparison of competing pathways are provided in the ESI (page S48 and Figure S51).

Conclusions

Mononuclear titanium and zirconium bis(aryloxide) complexes selectively catalyze the homogeneous transformation of N_2 to $HN(SiMe_3)_2$ in the presence of K^0, TMSCl, and weak acid at ambient temperature and pressure. The strong σ/π-donor aryloxide ligands stabilize the metal complex to the electrophilic reagents and facilitate binding and reduction of N_2. The Sm congener facilitates conversion of N_2 to $N(SiMe_3)_3$ but reacts too fast with the weak acid to catalyze the conversion to the bis(silyl)amine. The titanium catalyst **1Ti** is so stable that it can be reused multiple times, producing up to 51 eq. $HN(SiMe_3)_2$ over the course of four experiments. It is also a capable catalyst for the more difficult conversion of N_2 to ammonia. Most notably, like their dinuclear analogues **A-M**, mononuclear group 4 **1M** complexes only catalyze conversion of N_2 to $HN(SiMe_3)_2$; neither is competent for catalytic 3° silylamine production under our conditions. We suggest that steric constraints formed by the surrounding combination of aryloxides and K countercations around the 3d/4d metal cation prevents a third N-silylation, even without the formally defined cavity employed by group 4 **A-M**.

The similar catalytic yields of secondary silylamine obtained *per complex* using **1Ti** (26 eq. silylamine per complex) and **A-Ti** (30 eq. silylamine per complex) as N_2RR catalysts support the DOSY measurements and DFT-calculated mechanism invoking N_2 functionalization at a single Ti site. Here, DFT calculations again provide key insights into the mononuclear titanium-catalyzed dinitrogen silylation mechanism, reinforcing experimental observations, and highlighting the crucial role of potassium counterions, whose π-interactions with the ligand scaffold modulate both catalyst reactivity and the degree of amine substitution. Further, they identify the three-electron-reduced, non-deprotonated species **1Ti-N_2'** as an important intermediate in which three-electron reduction stabilizes the bound dinitrogen ligand while potassium counterions facilitate electron transfer and structural stabilization. The first replacement of a potassium cation with a proton is highly exergonic, and directs the catalyst selectivity for bis(silyl)amine. Then the exergonic release of $HN(SiMe_3)_2$ emerges as a critical driving force, ensuring efficient catalytic turnover. These findings establish a mononuclear, terminally bound N_2 activation mechanism, fully consistent with earlier studies that also indicated reaction progression primarily through a single titanium center. The evidence that when electropositive metal complexes can accommodate this atypical N_2 coordination geometry, they can function as effective N_2 reduction catalysts, and generate new amine products, offers a new approach to N2RR catalyst design for other parts of the periodic table such as the p-block, where current reports of N_2 binding are drawing increasing interest.

Materials and Methods

General Details

All manipulations were carried out under a dry, oxygen-free atmosphere of dinitrogen using standard Schlenk and glovebox techniques. Glassware, glass microfiber filters and cannulae were dried in an oven at 160 °C for at least 12 hours before use.

Solvents and Reagents

THF, hexanes, and toluene were collected from an MBraun Solvent Purification System packed with columns of activated alumina, degassed, and stored over activated 4 Å molecular sieves prior to use. Deuterated solvents were purchased from Cambridge Isotope Laboratories. C_6D_6, THF-d_8 and pyridine-d_5, and 2-MeTHF were refluxed over potassium, distilled, degassed, and stored on activated 4 Å molecular sieves prior to use. Pyridine was stirred over K^0, distilled, and degassed prior to use. DMSO-d_6 and d-chloroform were used as received.

All commercial solid reagents were used as purchased from Sigma Aldrich, following rigorous drying under dynamic vacuum. Na metal (ingot, 99.8 %) was brought into a glovebox, washed with hexanes, and thoroughly polished of any residual oxide and hydroxide coatings. K^0 metal (99.95 %) and Rb^0 metal (99.75 %) was used as received. KH was purchased as a dispersion in paraffin oil; the oil was washed away with hexane prior to use. Me_3SiCl and $Ti(OiPr)_4$ was degassed and distilled prior to use. $SmI_3(Et_2O)_{1.68}$, $CeI_3(Et_2O)_{0.66}$, $TiCl_4(THF)_2$, $TiCl_3(THF)_3$, $ZrBn_4$, KBn, KC_8, SmN''_3 (N ″ = $N(SiMe_3)_2$), CeN''_3, H_2DP^{Me2} ($(HOC_6H_2\text{-}^tBu_2\text{-}2,4)_2CMe_2$), $[HNEt_3][BPh_4]$, $[DNEt_3][BPh_4]$, and [HDBU][BPh_4] were prepared according to literature procedures. [46-49]

No uncommon hazards are noted.

Spectroscopy and Analytical Techniques

All NMR spectroscopic analyses were recorded at 298 K using Bruker AV-600, AVB-400, and AVQ-400 spectrometers. ^1H and ^{13}C NM[50]R spectra are referenced internally to the residual solvent ^1H and ^{13}C resonance respectively in deuterated solvents. Resonances are reported in parts per million (ppm). ^{15}N and ^{29}Si NMR spectra were referenced using an external standard of CH_3NO_2 (0.0 ppm) and $SiMe_4$ (0.0 ppm), respectively. Resonances are reported in parts per million (ppm).

ATR-FTIR spectra were recorded on a Shimadzu IRSpirit FTIR spectrometer on neat powders. Absorption bands are reported in wavenumbers (cm^{-1}) with a note on intensity: s – strong; m – medium; w – weak.

GC data were obtained by an Agilent Technologies 7890A GC System equipped with an Agilent 7693A Automatic Liquid Sampler. An Agilent VF-200ms GC column with dimensions 30 m × 0.25 mm × 0.25 μm was used. The sample injection temperature was 160 ºC. The method used an initial oven temperature of 50 ºC (held for 5 minutes), followed by a 20 ºC min-1 ramp to 160 ºC (held for 1 minute), followed by a 40 ºC min-1 ramp to 200 ºC (held for 1 minute). The retention times for the analytes of interest are as follows: 4.204 minutes for $HN(SiMe_3)_2$ and 9.273 minutes for $N(SiMe_3)_3$.

EPR experiments were carried out in the CalEPR center in the University of California, Davis. X-band continuous-wave spectra were recorded on the Bruker Biospin EleXsys E500 spectrometer equipped with a super high Q resonator (ER4122SHQE) and an ESR900 liquid helium cryostat with a temperature controller (Oxford Instrument ITC503), under slow-passage, non-saturating conditions. Spectrometer settings were as following: frequency = 9.4 GHz, conversion time = 60 ms, modulation amplitude = 0.5 mT, modulation frequency = 100 kHz.

Cyclic voltammetry (CV) experiments were performed under a dinitrogen atmosphere in a glovebox with an EC Epsilon (BASi) potentiostat, equipped with a 3 mm diameter glassy carbon working electrode, a Ag wire pseudoreference electrode, and a Pt wire counter electrode with either $[Bu_4N][PF_6]$ (0.1 M) or $[Bu_4N][BPh_4]$ supporting electrolyte solution in THF. The glassy carbon working electrode was cleaned prior to each experiment by polishing with Al_2O_3 (1 μm, 0.3 μm, 0.05 μm) in descending order and rinsed with ultrapure water and acetone before the measurements. All voltammograms were referenced to the Fc/Fc^+ or Fc^*/Fc^{*+} redox couple. Analyte concentrations were kept at 0.1 mM (**1Ti, 1Zr, 1Sm, 1Sm-I**) for the measurements.

Elemental analyses were carried out by Dr. Elena Kreimer and Dr. Ashleigh Lightbody at UC Berkeley.

X-ray crystallographic data for **1Ti**, **1Zr**, **1Sm-tol**, **1Sm-I**, **2Ti**, and **3Ti** were collected on a Rigaku XtaLAB Synergy-S diffractometer fitted with a HyPix-6000HE detector with Mo Kα radiation (λ = 0.71073 Å) or Cu Kα radiation (λ = 1.54184 Å) at 100 K. X-ray crystallographic data was collected on an Oxford Diffraction Excalibur Eos diffractometer with Mo Kα radiation (λ = 0.71073 Å) at 170 K. All structures were solved using SHELXT in Olex2 and refined using SHELXL in Olex2. Absorption corrections were completed using CrysAlis Pro (Rigaku Oxford Diffraction) software. Analytical numeric absorption corrections used a multifaceted crystal model based on expressions derived by Clark and Reid. Numerical absorption correction was based on a Gaussian integration over a multifaceted crystal model. Solvent accessible voids were treated using the Olex2 solvent mask S 6 function, and the final output of the mask was appended to the cif file and described in the additional details below.

Abbreviations:
' = $SiMe_3$
HN" = $HN(SiMe_3)_2$
N"' = $N(SiMe_3)_3$
eq. = equivalent
2-Me-THF = 2-methyltetrahydrofuran
Fc = ferrocene
Fc^* = decamethylferrocene
DBU = 1,8-Diazabicyclo[5.4.0]undec-7-ene
DP = diphenolate
*m*TP = *meta*-tetraphenolate

Syntheses

$(HOC_6H_2$-^{t}Bu-2,Me-4)$_2$CHPh, **H_2DP**

Modification of a literature procedure.[21]

A Schlenk flask equipped with a magnetic stir bar and oil bubbler was charged with 2-*tert*-butyl-4-methylphenol (5.0224 g, 30.580 mmol, 2.2 eq.), benzaldehyde (1.418 mL, 13.900 mmol, 1 eq.), and *p*-toluenesulfonic acid monohydrate (264 mg, 1.3900 mmol, 0.1 eq.). The flask was placed under nitrogen flow, stirred, and heated to 75 °C. The solids melted to yield a brown solution which darkened over time. After *circa* 16 hours, the reaction mixture had turned into a reddish-white solid at which point 50 mL of MeCN was added. The resulting brown suspension was filtered to provide $(HOC_6H_2$-^{t}Bu-2,Me-4)$_2$CHPh as a colorless solid which was washed with additional MeCN. The solid was dried under vacuum at 70 °C overnight and stored in a glovebox, and characterized as HOC_6H_2-^{t}Bu-2,Me-4)$_2$CHPh, **H_2DP**, $C_{29}H_{36}O_2$. Yield 3.4745 g (60 %).

$(HOC_6H_2$-^{t}Bu-2,Me-4)$_2$CMePh, **H_2DP^{Me}**

Prepared according to a literature procedure.[34]

Ti(DP)$_2$, **1Ti**

To a magnetically stirred toluene solution (4 mL) of **H_2DP** (167.5 mg, 0.4021 mmol, 2 eq.) was added Ti(O^{i}Pr)$_4$ (60.0 mg, 0.2111 mmol, 1.05 eq.) dropwise in toluene (1 mL). The resulting transparent orange-red solution was stirred at reflux in a teflon-tapped ampoule under at atmosphere of N_2 for 16 hours. The volatiles were removed *in vacuo* resulting in the recovery of a yellow-orange solid. The solid was repeatedly washed with cold hexanes (5 x 1 mL) to give Ti[CHPh(OC$_6$H$_2$-^{t}Bu-2,Me-4)$_2$]$_2$, **1Ti**, as a bright yellow-orange powder. (159.2 mg, 0.1815 mmol, 90% yield). The compound is stable to air both in the solid and solution phase for several hours. Single crystals can be grown from a room temperature solution of the solid in 1:1 n-hexane/toluene. **^{1}H NMR** (500 MHz, C_6D_6 25°C) δ 7.47 (d, *J* = 8.4 Hz, 4H, Ar*H*), 7.35 (d, *J* = 2.4 Hz, 2H, Ar*H*), 7.28 (d, *J* = 2.4 Hz, 2H, Ar*H*), 7.09 (m, *J* = 7.2 Hz, 6H; overlapping resonances, Ar*H*), 7.03 (t, *J* = 6.6 Hz, 2H, Ar*H*), 6.92 (d, *J* = 2.4 Hz, 2H, Ar*H*), 6.63 (s, 2H, Ar$_3$C*H*), 2.12 (s, 6H, ArCH_3), 1.97 (s, 6H, ArCH_3), 1.54 (s, 18H, ArCMe_3), 1.38 (s, 18H, ArCMe_3). **^{13}C{^{1}H} NMR** (151 MHz, C_6D_6, 25°C) δ 161.67, 160.55, 143.25, 139.31, 136.73, 136.32, 134.75, 132.04, 131.85, 130.63, 128.47, 128.15, 126.58, 126.42, 126.36, 47.25, 35.64, 35.26, 30.85, 30.71, 21.33, 21.23. **Elemental analysis** (%) calc. for $C_{58}H_{68}O_4Ti$ (877.04 g·mol^{-1}): C, 79.43; H, 7.82. Found: C, 78.79; H, 7.96.

Ti(DP^{Me})$_2$, **1Ti^{Me}**

To a magnetically stirred THF solution (2 mL) of **H_2DP^{Me}** (217.1 mg, 0.480 mmol, 2 eq.) was slowly added a THF slurry (2 mL) of KH (38.5 mg, 0.959 mmol, 4 eq.). The mixture was allowed to stir for 45 min to ensure stoichiometric deprotonation, then a yellow THF slurry (4 mL) of $TiCl_4(THF)_2$ (80.1 mg, 0.240 mmol, 1 eq.) was added dropwise to the colorless solution of K_2DP^{Me}. The reaction mixture was allowed to stir at room temperature for 3 h, during which time the yellow color deepened. The product mixture was concentrated *in vacuo* and filtered to remove KCl. The filtrate was dried *in vacuo* and washed with hexanes (2 mL) to afford Ti(DP^{Me})$_2$, **1Ti^{Me}** as a yellow powder (119 mg, 0.125 mmol, 52.3% yield). Single crystals were grown from a saturated pyridine solution of the product stored at -35°C. **^{1}H NMR** (500 MHz, d$_5$-Pyr, 25°C) δ 7.78 (s, 2H, Ar*H*) 7.48 (s, 2H, Ar*H*), 7.24 (s, 2H, Ar*H*), 7.23 (s, 2H, Ar*H*), 2.50 (s, 6H, -CMe_2-), 1.98 (s, 6H, -CMe_2-), 1.96

(s, 18H, ArC*Me*$_3$), 1.62 (s, 18H, ArC*Me*$_3$), 1.47 (s, 18H, ArC*Me*$_3$), 1.24 (s, 18H, ArC*Me*$_3$). **^{13}C{^{1}H} NMR** (126 MHz, d_5-pyr, 25°C) δ 167.05, 164.78, 141.59, 139.20, 137.58, 137.50, 137.17, 121.43, 120.70, 119.41, 71.94, 68.29, 47.04, 43.67, 43.36, 37.91, 36.69, 36.59, 35.22, 35.04, 34.89, 34.67, 33.06, 32.81, 32.52, 32.13, 32.03, 30.81, 28.96, 26.27, 23.30, 14.69. **Elemental analysis** (%) calc. for $C_{62}H_{92}O_4Ti$ (949.28 gmol^{-1}): C, 78.45; H, 9.77. Found: C, 68.15; H, 8.98. **HRMS** (ESI, positive): *m/z* 949.6628 (calc for [M+H$^+$] 949.6553).

[KTi(DP)$_2$(THF)$_2$], **2Ti**

To a magnetically stirred THF solution (2 mL) of **H_2DP** (99.9 mg, 0.240 mmol, 2 eq.) was slowly added a THF slurry (2 mL) of KH (19.2 mg, 0.480 mmol, 4 eq.). The mixture was allowed to stir for 30 min to ensure stoichiometric deprotonation, then a blue THF suspension (4 mL) of $TiCl_3(THF)_3$ (44.4 mg, 0.120 mmol, 1 eq.) was added dropwise to the colorless solution. The reaction mixture was allowed to stir at room temperature for 16 h, during which time the color changed from blue to yellow, then to red-brown. The product mixture was concentrated *in vacuo* and filtered to remove KCl. Diffusion of n-hexane vapor into a concentrated THF solution of the filtrate afforded [KTi(DP)$_2$(THF)$_2$], **2Ti** as yellow crystals that were suitable for SCXRD. (77.9 mg, 0.0735 mmol, 61.2% yield). **^{1}H NMR** (500 MHz, d_8-THF, 25°C) δ 11.10, 7.27, 6.97, 6.63, 4.50, 3.83, 3.62 (m, 8H; 2 THF *CH*$_2$) 2.80, 1.77 (m, 8H; 2 THF *CH*$_2$), 1.73, 1.55. **Elemental analysis** (%) calc. for $C_{66}H_{84}O_6KTi$ (1060.36 g·mol^{-1}): C, 74.76; H, 7.99. Found: C, 75.42; H, 8.23. **EPR** g = [2.00, 1.95, 1.93]

[K_3Ti(DP$^-$)$_2$(THF)$_2$], **3Ti**

To a stirring solution of **2Ti** (100.0 mg, 0.094 mmol) in THF (2 mL) was added KC_8 (25.5 mg, 0.189 mmol, 2 equiv.) suspended in THF (2 mL). The resulting suspension was stirred at room temperature overnight. The mixture was filtered through a glass microfiber plug and the resulting red solution was collected. The volatiles were removed in vacuo and the solids were redissolved in THF (1.5 mL). Hexanes (1 mL) were layered on top of this solution and allowed to stand at -38°C undisturbed overnight after which point large red crystals of the product had formed, suitable for SCXRD. The mother liquor was decanted off and the red crystals were washed with a 1:1 THF:hexanes mixture followed by an additional aliquot of hexanes. After removal of all volatiles in vacuo, the K_3[Ti(DP$^-$)$_2$(THF)$_2$] product was isolated as a dark-red powder (58.1 mg, 0.0511 mmol, 54.2 % yield). **^{1}H NMR** (500 MHz, d_8-THF, 25°C) δ 13.39, 9.04, 6.23, 3.62 (m, 8H; 2 THF C*H*$_2$), 1.78 (m, 8H; 2 THF C*H*$_2$), 0.56, -4.94, -11.93.

^{13}C{^{1}H} NMR δ 140.57, 122.18, 91.06, 68.39, 68.10, 39.72, 33.56, 32.70, 30.65, 30.44, 26.55, 25.98, 23.69, 18.11, 14.59. **Elemental analysis** (%) calc. for $C_{66}H_{82}O_6K_3Ti$ (1163.54 g·mol^{-1}): C, 69.75; H, 7.27. Found: C, 68.80; H, 7.24. **EPR** g = [1.98, 1.92, 1.74]

Zr(DP)$_2$, **1Zr**

To a magnetically stirred toluene (2 mL) solution of H_2DP (62.8 mg, 0.151 mmol, 2 eq.) was added $ZrBn_4$ (34.4 g, 0.0755 mmol, 1 eq.) dropwise in toluene (2 mL). The resulting brown solution was stirred at room temperature in a 20 mL scintillation vial inside an N_2-filled glovebox for 16 hours. The volatiles were removed *in vacuo* to afford an off-white solid. The solid was recrystallized from

a saturated toluene solution at -35°C to give $Zr(DP)_2$, **1Zr**, as colorless crystals suitable for SCXRD. (29.4 mg, 0.0292 mmol, 38.7 % yield). **^{1}H NMR** (400 MHz, C_6D_6, 25°C) δ 7.45 (d, *J* = 7.6 Hz, 4H, Ar*H*), 7.36 (s, 2H, Ar*H*), 7.31 (s, 2H, Ar*H*), 7.13 – 7.07 (m, 6H, Ar*H*), 7.03 (t, *J* = 7.2 Hz, 2H, Ar*H*), 6.98 (s, 2H, Ar*H*), 6.08 (s, 2H, Ar_3C*H*), 2.12 (s, 6H, ArC*Me*), 2.03 (s, 6H, ArC*Me*), 1.51 (s, 18H, ArC*Me$_3$*), 1.36 (s, 18H, ArC*Me$_3$*). **^{13}C{^{1}H} NMR** (160 MHz, C_6D_6, 25°C) δ 157.45, 137.48, 137.09, 130.37, 126.86, 126.67, 126.61, 35.42, 35.24, 30.78, 30.53, 21.29, 21.26. **Elemental analysis** (%) calc. for $C_{64}H_{82}O_4Zr$ (1006**.**58 g·mol^{-1}): C, 76.37; H, 8.21. Found: C, 76.17; H, 8.11.

$KSm(DP)_2(THF)_3$, **1Sm**

To a magnetically stirred THF (5 mL) solution of H_2DP (311.6 mg, 0.748 mmol, 2 eq.) first was added a THF solution (3 mL) of $Sm(N(SiMe_3)_2)_3$ (236.2 mg, 0.3740 mmol, 1 eq.), followed by a THF solution of $KN(SiMe_3)_2$ (74.6 mg, 0.3740 mmol, 1 eq.). The resulting pink solution was stirred at room temperature in a 20 mL scintillation vial inside an N_2-filled glovebox for 16 hours, during which time a colorless solid precipitated from solution. The precipitate was isolated by filtration on a fine-porosity glass fritted funnel and washed with 5 x 1 mL portions of THF to yield $KSmDP_2(THF)_3$ as a colorless powder which was further dried *in vacuo* for several hours (435.7 mg, 0.3528 mmol, 94.3 % yield). Single crystals of the toluene adduct **1Sm-tol,** characterized as $KSmDP_2(PhMe)_2$, can be grown from a concentrated toluene product solution at -35°C of an identical procedure to that described for 1Sm but performed in toluene. **^{1}H NMR** (500 MHz, d_5-pyr, 25°C) δ 8.90 (4H, Ar*H*), 7.84 (4H, Ar*H*), 6.70 (4H, Ar*H*), 6.45 (6H, Ar*H*), 5.02 (2H, Ar_3C*H*), 3.66 (m, 12H; 3 THF C*H$_2$*), 2.86 (12H, Ar*Me*), 1.62 (m, 12H; 3 THF C*H$_2$*), 1.38 (36H, ArC*Me$_3$*). **^{13}C{^{1}H} NMR** (126 MHz, d_5-pyr, 25°C) δ 139.40, 136.50, 131.12, 130.12, 129.65, 128.90, 126.63, 126.05, 121.40, 68.07, 36.84, 31.64, 26.05, 22.86. **Elemental analysis** (%) calc. for $C_{70}H_{92}O_7KSm$ (1234.96 g·mol^{-1}): C, 68.08; H, 7.51. Found: C, 64.7; H, 7.11.

$SmI(DP)(THF)_3$, **1Sm-I**

To a magnetically stirred THF solution (2 mL) of H_2DP (64.3 mg, 0.154 mmol, 1 eq.) was added a THF solution (2 mL) of $KN(SiMe_3)_2$ (61.6 mg, 0.309 mmol, 2 eq.). The colorless, homogeneous reaction mixture was allowed to stir for 1 hour, after which time the solution was added dropwise to a magnetically stirred yellow-green THF slurry of $SmI_3(Et_2O)_x$ (94.2 mg, 0.154 mmol, 1 eq.). The reaction mixture was allowed to stir at ambient temperature for 16 hours then filtered through a glass fiber pipette filter. The yellow filtrate was dried *in vacuo* and the resulting solid was washed with hexanes (3 x 1 mL). The solids were resuspended in THF and filtered again through a glass fiber pipette filter. The filtrate was concentrated and subjected to slow vapor diffusion of hexanes, which afforded crystals suitable for SCXRD (104.8 mg, 0.131 mmol, 85.1% yield). **^{1}H NMR** (500 MHz, d_8-THF, 25°C) δ 8.85 (s, 1H, Ar_3C*H*), 7.77 (s, 2H, Ar*H*), 7.20 (d, 2H, Ar*H*), 7.09 (s, 2H, Ar*H*), 6.97 (t, 2H, Ar*H*), 6.85 (t, 1H, Ar*H*), 3.62 (m, 12H; 3 THF C*H$_2$*), 2.32 (s, 6H, Ar*Me*), 1.98 (s, 18H, ArC*Me$_3$*), 1.78 (m, 12H; 3 THF C*H$_2$*). **^{13}C{^{1}H} NMR** (126 MHz, d_8-THF, 25°C) δ 165.20, 149.66, 135.69, 134.19, 131.03, 130.44, 128.00, 126.13, 125.36, 125.08, 68.38, 49.07, 37.47, 31.74, 26.54, 22.30.

Elemental analysis (%) calc. for $C_{35}H_{44}O_{3.5}ISm$ (800.00 g·mol^{-1}): C, 52.54; H, 5.56. Found: C, 51.7; H, 5.75.

$K_3Ti(DP)(DP^-)(N_2)(THF)$, **1Ti-$N_2$**

To a stirred solution of **2Ti** (15.3 mg, 0.0144 mmol) in THF (2 mL) at -78°C was added KC_8 (19.5 mg, 0.144 mmol, 10 eq.) suspended in THF (2 mL) also at -78°C inside an N_2-filled glovebox. The resulting mixture was allowed to warm to room temperature overnight with stirring, then filtered through a glass microfiber plug to collect the resulting red solution. The volatiles were removed under reduced pressure and the solids were washed with hexanes (2 mL). After removal of all volatiles under reduced pressure, $K_3Ti(DP^-)(DP)_2(N_2)(THF)$, **1Ti-$N_2$** was isolated as a dark-red powder (16.7 mg, 0.0144 mmol, 99% yield). This compound can also be prepared from **1Ti** as the starting material via an analogous procedure in slightly lower yields. **^{1}H NMR** (600 MHz, d_8-THF, 25°C) δ 7.20 (d, 2H, Ar*H*), 7.06 (t, 2H, Ar*H*), 6.93 (t, 1H, Ar*H*), 6.79 (s, 1H, Ar*H*), 6.74 (d, 1H, Ar*H*), 6.60 (d, 2H, Ar*H*), 6.58 (d, 1H, Ar*H*), 6.50 (d, 2H, Ar*H*), 6.44 (s, 1H, Ar*H*), 6.34 (d, 2H, Ar*H*), 6.27 (t, 2H, Ar*H*), 6.00 (broad s, 1H, Ar_3CH), 5.02 (1H, m), 3.62 (m, 4H; THF CH_2), 2.03-1.99 (ArCH_3, 12 H), 1.77 (m, 4H; THF CH_2), 1.37-1.32 (ArCMe_3, 36H). **^{13}C{^{1}H} NMR** (126 MHz, d_8-THF, 25°C) δ 168.084, 167.116, 166.458, 151.084, 136.485, 135.919, 134.943, 131.347, 129.838, 129.743, 129.469, 129.074, 128.021, 126.209, 124.714, 119.967, 114.519, 68.386, 68.101, 43.872, 35.920, 35.767, 32.708, 30.775, 30.698, 26.554, 23.693, 21.888, 21.698, 21.471, 14.593.

Elemental analysis (%) calc. For $C_{66}H_{84}K_3N_2O_6Ti$ (1093.46 $gmol^{-1}$): C, 67.95; H, 7.26; N, 2.4. Found: C, 58.21; H, 6.09; N, 1.09. **EPR** g = 2.003.

1Ti-$^{15}N_2$

The ^{15}N-labeled complex **1Ti-$^{15}N_2$** is made in an identical manner to that of **1Ti-N_2**, except under a $^{15}N_2$ atmosphere. A ^{1}H NMR spectrum of the **1Ti-$^{15}N_2$** is shown in Figure S21, but ^{15}N NMR spectroscopy of 5 mM solution of **1Ti-$^{15}N_2$** gave no measurable resonance within a spectral window of –4000 to 4000 ppm.

Supporting Information:

Additional experimental details, materials and methods, NMR spectra, electrochemical data, crystallographic data, EPR spectra. Open data are at doi: 10.17632/949k3hnwsm.1.

Acknowledgements

The syntheses were supported by the National Science Foundation (NSF, CHE-2348646). The catalysis studies were supported by the Catalysis Program, FWP CH030201, in the U.S. Department of Energy (DOE), Office of Science, Office of Basic Energy Sciences, Chemical Sciences, Geosciences, and Biosciences Division, at the Lawrence Berkeley National Laboratory. The Catalysis Laboratory in the DOE Catalysis Program also provided resource and instrumentation used in this work. All of these DOE programs and facilities operate under contract no. DE-AC02- 05CH11231. EPR spectroscopic studies were funded by the National Institutes of Health (NIH R35 grant 1R35GM126961 to RDB). Computational analyses on mechanism were supported by the UK EPSRC, EPX0420491 (NK, PLA). DE-SC0021266. We thank the Pines Center and Hasan Celik for NMR spectroscopic support and discussions and the National Institutes

of Health (NIH) for funding the UC Berkeley College of Chemistry NMR facility under grant no 1S10RR016634-01. We thank the University of Manchester for its Computational Shared Facility (CSF3, CSF4) and associated support services.

Conflict of Interest

An international patent application has been filed with the US receiving office, PCT/US23/74839.

Supplementary data available

Full experimental and characterizing date in PDF format. Crystallographic CIF data are deposited with the CCDC under codes 2512842-2512847, 2550574.

References

(1) Shiina, K. Reductive silylation of molecular nitrogen via fixation to tris(trialkylsilyl)amine. *J. Am. Chem. Soc.* **1972**, *94* (26), 9266–9267. DOI: 10.1021/ja00781a068.

(2) Wong, A.; Lam, F. Y. T.; Hernandez, M.; Lara, J.; Trinh, T. M.; Kelly, R. P.; Ochiai, T.; Rao, G.; Britt, R. D.; Kaltsoyannis, N.; et al. Catalytic reduction of dinitrogen to silylamines by earth-abundant lanthanide and group 4 complexes. *Chem Catal.* **2024**, *4* (5), 100964. DOI: 10.1016/j.checat.2024.100964

(3) Imayoshi, R.; Nakajima, K.; Nishibayashi, Y. Vanadium-catalyzed reduction of molecular dinitrogen into silylamine under ambient reaction conditions. *Chem. Lett.* **2017**, *46* (4), 466–468.

(4) Li, Z.; Liu, C.; An, J.; Wang, X.; Hu, S. Catalytic Dinitrogen Reduction to Silylamines by Molybdenum Nitride Complexes Bearing a Diphenolate N-Heterocyclic Carbene Ligand. *ACS Catalysis* **2024**, *14* (9), 6558–6564. DOI: 10.1021/acscatal.4c00307.

(5) Imayoshi, R.; Tanaka, H.; Matsuo, Y.; Yuki, M.; Nakajima, K.; Yoshizawa, K.; Nishibayashi, Y. Cobalt-Catalyzed Transformation of Molecular Dinitrogen into Silylamine under Ambient Reaction Conditions. *Chem. Eur. J.* **2015**, *21* (24), 8905–8909. DOI: 10.1002/chem.201501088 .

(6) Arnold, P. L.; Ochiai, T.; Lam, F. Y. T.; Kelly, R. P.; Seymour, M. L.; Maron, L. Metallacyclic actinide catalysts for dinitrogen conversion to ammonia and secondary amines. *Nature Chem.* **2020**, *12* (7), 654–659. DOI: 10.1038/s41557-020-0457-9.

(7) Yamout, L. S.; Ataya, M.; Hasanayn, F.; Holland, P. L.; Miller, A. J. M.; Goldman, A. S. Understanding Terminal versus Bridging End-on N2 Coordination in Transition Metal Complexes. *Journal of the American Chemical Society* **2021**, *143* (26), 9744–9757. DOI: 10.1021/jacs.1c01146.

(8) Burford, R. J.; Fryzuk, M. D. Examining the relationship between coordination mode and reactivity of dinitrogen. *Nature Reviews Chem.* **2017**, *1*, 0026, DOI: 10.1038/s41570-017-0026.
(9) Komori, K.; Oshita, H.; Mizobe, Y.; Hidai, M. Preparation and properties of molybdenum and tungsten dinitrogen complexes. 25. Catalytic conversion of molecular nitrogen into silylamines using molybdenum and tungsten dinitrogen complexes. *Journal of the American Chemical Society* **1989**, *111* (5), 1939–1940. DOI: 10.1021/ja00187a092.
(10) Kuriyama, S.; Nishibayashi, Y. Development of catalytic nitrogen fixation using transition metal complexes not relevant to nitrogenases. *Tetrahedron* **2021**, *83*, 131986. DOI: https://doi.org/10.1016/j.tet.2021.131986.
(11) Singh, D.; Buratto, W. R.; Torres, J. F.; Murray, L. J. Activation of Dinitrogen by Polynuclear Metal Complexes. *Chemical Reviews* **2020**, *120* (12), 5517–5581. DOI: 10.1021/acs.chemrev.0c00042.
(12) Burford, R. J.; Yeo, A.; Fryzuk, M. D. Dinitrogen activation by group 4 and group 5 metal complexes supported by phosphine-amido containing ligand manifolds. *Coord. Chem. Rev.* **2017**, *334*, 84–99. DOI: https://doi.org/10.1016/j.ccr.2016.06.015.
(13) Evans, W. J.; Lee, D. S.; Rego, D. B.; Perotti, J. M.; Kozimor, S. A.; Moore, E. K.; Ziller, J. W. Expanding Dinitrogen Reduction Chemistry to Trivalent Lanthanides via the LnZ3/Alkali Metal Reduction System: Evaluation of the Generality of Forming Ln2(μ-η2:η2-N2) Complexes via LnZ3/K. *Journal of the American Chemical Society* **2004**, *126* (44), 14574–14582. DOI: 10.1021/ja046047s.
(14) Shivaraam, R. A. K.; Rajeshkumar, T.; Scopelliti, R.; Živković, I.; Maron, L.; Mazzanti, M. Dinitrogen Reduction and Functionalization by a Siloxide Supported Thulium-Potassium Complex for the Formation of Ammonia or Hydrazine Derivatives. *Angewandte Chemie International Edition* **2025**, *64* (1), e202414051. DOI: https://doi.org/10.1002/anie.202414051.
(15) Connor, G. P.; Holland, P. L. Coordination chemistry insights into the role of alkali metal promoters in dinitrogen reduction. *Catal. Today* **2017**, *286*, 21–40. DOI: https://doi.org/10.1016/j.cattod.2016.08.014.
(16) Tanabe, Y.; Nishibayashi, Y. Recent advances in catalytic silylation of dinitrogen using transition metal complexes. *Coord. Chem. Rev.* **2019**, *389*, 73–93. DOI: 10.1016/j.ccr.2019.03.004.
(17) Duman, L. M.; Sita, L. R. Closing the Loop on Transition-Metal-Mediated Nitrogen Fixation: Chemoselective Production of $HN(SiMe_3)_2$ from N_2, Me_3SiCl, and X—OH (X = R, R_3Si, or Silica Gel). *J. Am. Chem. Soc.* **2017**, *139* (48), 17241–17244. DOI: 10.1021/jacs.7b08859.

(18) Mori, M. Activation of nitrogen for organic synthesis. *Journal of Organometallic Chemistry* **2004**, *689* (24), 4210–4227. DOI: https://doi.org/10.1016/j.jorganchem.2004.05.053.
(19) Inamoto, K.; Okawa, H.; Taneda, H.; Sato, M.; Hirono, Y.; Yonemoto, M.; Kikkawa, S.; Kondo, Y. Organocatalytic deprotonative functionalization of C(sp2)–H and C(sp3)–H bonds using in situ generated onium amide bases. *Chemical Communications* **2012**, *48* (78), 9771–9773, 10.1039/C2CC35701A. DOI: 10.1039/C2CC35701A.
(20) Shigeno, M.; Kajima, A.; Nakaji, K.; Nozawa-Kumada, K.; Kondo, Y. Catalytic amide base system generated in situ for 1,3-diene formation from allylbenzenes and carbonyls. *Org. Biomol. Chem.* **2021**, *19* (5), 983–987, 10.1039/D0OB02007A.
(21) Wells, J. A. L.; Seymour, M. L.; Suvova, M.; Arnold, P. L. Dinuclear uranium complexation and manipulation using robust tetraaryloxides. *Dalton Trans.* **2016**, *45* (40), 16026–16032, 10.1039/C6DT02630C..
(22) Arnold, P. L.; Wang, K.; Gray, S. J.; Moreau, L. M.; Booth, C. H.; Curcio, M.; Wells, J. A. L.; Slawin, A. M. Z. Dicerium letterbox-shaped tetraphenolates: f-block complexes designed for two-electron chemistry. *Dalton Trans.* **2020**, *49* (3), 877–884, 10.1039/C9DT03291F.
(23) Amonoo-Neizer, E. H.; Shaw, R. A.; Skovlin, D. O.; Smith, B. C.; Rosenthal, J. W.; Jolly, W. L. Lithium Bis(trimethylsilyl)amide and Tris(trimethylsilyl)amine. In *Inorganic Syntheses*, 1966; pp 19–22.
(24) Anderson, B. A. Hexamethyldisilazane. In *Encyclopedia of Reagents for Organic Synthesis*.
(25) Shayapov, V. R.; Rumyantsev, Y. M.; Dzyuba, A. A.; Ayupov, B. M.; Fainer, N. I. Mechanical stresses in silicon carbonitride films obtained by PECVD from hexamethyldisilazane. *Appl. Surf. Sci.* **2013**, *265*, 385–388. DOI: https://doi.org/10.1016/j.apsusc.2012.11.017.
(26) Ahmad, S.; Arnold, P. L.; Kaltsoyannis, N. Electron–Electrophile Coupled Dinitrogen Reduction in a Cerium–Meta-Tetraphenolate System: A Computational Study [Manuscript submitted for publication]. **2026**.
(27) Bercaw, J. E. Bis(pentamethylcyclopentadienyl)titanium(II) and its complexes with molecular nitrogen. *JACS* **1974**, *96* (16), 5087–5095. DOI: 10.1021/ja00823a012 (accessed 2024/09/17/01:33:07). From ACS Publications.
(28) Hanna, T. E.; Lobkovsky, E.; Chirik, P. J. Dinitrogen Activation by Titanium Sandwich Complexes. *JACS* **2004**, *126* (45), 14688–14689. DOI: 10.1021/ja045884r.
(29) Chirik, P. J. Dinitrogen functionalization with bis(cyclopentadienyl) complexes of zirconium and hafnium. *Dalton Trans.* **2007**, (1), 16–25, 10.1039/B613514E. DOI: 10.1039/B613514E.

(30) Singh, A.; Moore, C. E.; Thomas, C. M. Side-On N2 Binding and Reduction by a Heterotetrametallic Zr2Co2 Cluster. *JACS* **2025**, *147* (44), 40087–40092. DOI: 10.1021/jacs.5c14342.
(31) Singh, D.; Buratto, W. R.; Torres, J. F.; Murray, L. J. Activation of Dinitrogen by Polynuclear Metal Complexes. *Chem. Rev.* **2020**, *120* (12), 5517–5581. DOI: 10.1021/acs.chemrev.0c00042.
(32) Karraker, D. G. Coordination of trivalent lanthanide ions. *J. Chem. Educ.* **1970**, *47* (6), 424. DOI: 10.1021/ed047p424.
(33) Shannon, R. Revised effective ionic radii and systematic studies of interatomic distances in halides and chalcogenides. *Acta Cryst. A* **1976**, *32* (5), 751–767. DOI: 10.1107/S0567739476001551.
(34) Söhner, T.; Küppers, I. K.; Wackerow, W.; Rominger, F.; Straub, B. F. Synthesis and structure of salts of a sterically shielded, lipophilic, C2-symmetric, fluxional aluminate. *Arkivoc* **2014**, *2014* (4), 296–318. DOI: 10.3998/ark.5550190.p008.404.
(35) Evans, D. F. 400. The determination of the paramagnetic susceptibility of substances in solution by nuclear magnetic resonance. *J. Chem. Soc.* **1959**, (0), 2003–2005, 10.1039/JR9590002003.
(36) Ghana, P.; van Krüchten, F. D.; Spaniol, T. P.; van Leusen, J.; Kögerler, P.; Okuda, J. Conversion of dinitrogen to tris(trimethylsilyl)amine catalyzed by titanium triamidoamine complexes. *Chem. Commun.* **2019**, *55* (22), 3231–3234, 10.1039/C8CC09742A.
(37) Doyle, L. R.; Wooles, A. J.; Jenkins, L. C.; Tuna, F.; McInnes, E. J. L.; Liddle, S. T. Catalytic Dinitrogen Reduction to Ammonia at a Triamidoamine–Titanium Complex. *Angewandte Chemie International Edition* **2018**, *57* (21), 6314–6318. DOI: 10.1002/anie.201802576.
(38) Wu, B.; Chen, W.; Yan, H.; Zhang, X.; Wei, J.; Xi, Z.; Wang, G.-X.; Ye, S. Trisilylation of a Formal Cr(-I) Bis-dinitrogen Complex. *JACS* **2025**, *147* (36), 32480–32493. DOI: 10.1021/jacs.5c05591.
(39) Ohki, Y.; Fryzuk, M. D. Dinitrogen Activation by Group 4 Metal Complexes. *Angewandte Chemie International Edition* **2007**, *46* (18), 3180–3183. DOI: https://doi.org/10.1002/anie.200605245.
(40) Nakanishi, Y.; Ishida, Y.; Kawaguchi, H. Nitrogen–Carbon Bond Formation by Reactions of a Titanium–Potassium Dinitrogen Complex with Carbon Dioxide, tert-Butyl Isocyanate, and Phenylallene. *Angewandte Chemie International Edition* **2017**, *56* (31), 9193–9197. DOI: 10.1002/anie.201704286.
(41) Hanna, T. E.; Bernskoetter, W. H.; Bouwkamp, M. W.; Lobkovsky, E.; Chirik, P. J. Bis(cyclopentadienyl) Titanium Dinitrogen Chemistry: Synthesis and Characterization of a Side-on Bound Haptomer. *Organometallics* **2007**, *26* (9), 2431–2438. DOI: 10.1021/om0611913.

(42) Yin, Z.-B.; Wang, G.-X.; Yan, X.; Wei, J.; Xi, Z. Construction of N-E bonds via Lewis acid-promoted functionalization of chromium-dinitrogen complexes. *Nature Commun.* **2025**, *16* (1), 674. DOI: 10.1038/s41467-025-55998-5.
(43) Wang, G.-X.; Yin, Z.-B.; Wei, J.; Xi, Z. Dinitrogen Activation and Functionalization Affording Chromium Diazenido and Hydrazido Complexes. *Acc. Chem. Res.* **2023**, *56* (22), 3211–3222. DOI: 10.1021/acs.accounts.3c00476.
(44) Tanabe, Y.; Nishibayashi, Y. Recent advances in nitrogen fixation upon vanadium complexes. *Coord. Chem. Rev.* **2019**, *381*, 135–150. DOI: https://doi.org/10.1016/j.ccr.2018.11.005.
(45) Holland, P. L. Metal–dioxygen and metal–dinitrogen complexes: where are the electrons? *Dalton Transactions* **2010**, *39* (23), 5415–5425, 10.1039/C001397H.
(46) Gompa, T. P.; Rice, N. T.; Russo, D. R.; Aguirre Quintana, L. M.; Yik, B. J.; Bacsa, J.; La Pierre, H. S. Diethyl ether adducts of trivalent lanthanide iodides. *Dalton Trans.* **2019**, *48* (23), 8030–8033, 10.1039/C9DT00775J.
(47) Jones, N. A.; Liddle, S. T.; Wilson, C.; Arnold, P. L. Titanium(III) alkoxy-N-heterocyclic carbenes and a safe, low-cost route to $TiCl_3(THF)_3$. *Organometallics* **2007**, *26* (3), 755–757. DOI: 10.1021/om060486d.
(48) Wang, K.-T.; Wang, Y.-X.; Wang, B.; Li, Y.-G.; Li, Y.-S. Novel zirconium complexes with constrained cyclic β-enaminoketonato ligands: improved catalytic capability toward ethylene polymerization. *Dalton Trans.* **2016**, *45* (25), 10308–10318, 10.1039/C6DT01391K.
(49) Görl, C.; Betthausen, E.; Alt, H. G. Di- and trinuclear iron/titanium and iron/zirconium complexes with heterocyclic ligands as catalysts for ethylene polymerization. *Polyhedron* **2016**, *118*, 37–51. DOI: https://doi.org/10.1016/j.poly.2016.07.033.
(50) Gande, V. V.; Kani, N. C.; Goyal, I.; Chauhan, R.; Qi, Y.; Olusegun, S. A.; Gauthier, J. A.; Singh, M. R. Advancements in dinitrogen activation for catalytic breakthroughs. *EES Catalysis* **2025**, *3* (5), 883–920, 10.1039/D5EY00033E.

Summary picture

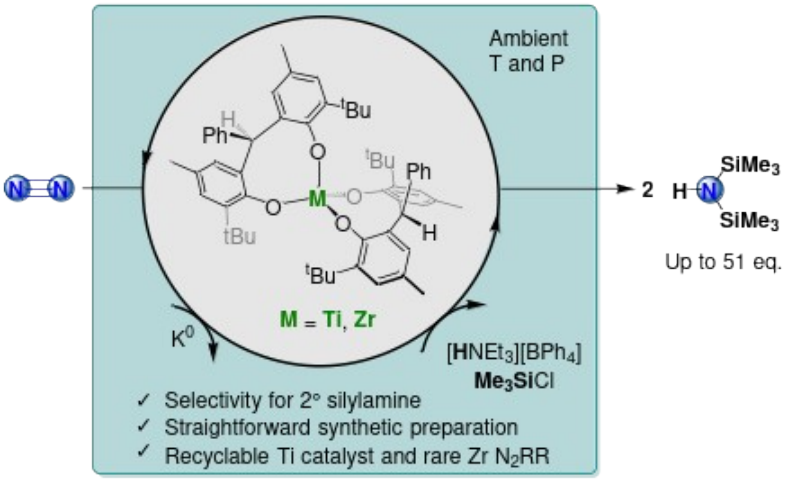
Ambient
T and P
tBu
Ph
H
O
tBu
Ph
M
O
O
tBu
H
tBu
M = Ti, Zr
K0
[HNEt3][BPh4]
Me3SiCl
2
SiMe3
H
N
SiMe3
Up to 51 eq.
✓ Selectivity for 2° silylamine
✓ Straightforward synthetic preparation
✓ Recyclable Ti catalyst and rare Zr N2RR